

# Design Concepts for Peel-Dominant Adhesive Joints in Aeronautic Applications

J.P.M. Lopes<sup>1</sup>, R.D.S.G. Campilho<sup>1,2,\*</sup>, M.A. Bellali<sup>3</sup> and M. Baghdadi<sup>3</sup>

<sup>1</sup>ISEP – School of Engineering, Polytechnic of Porto, Rua Dr. António Bernardino de Almeida, 431, 4200-072 Porto, Portugal

<sup>2</sup>INEGI – Pólo FEUP, Rua Dr. Roberto Frias, s/n, 4200-465 Porto, Portugal

<sup>3</sup>Laboratory of Physical Mechanics of Materials (LMPM), Djillali Liabes University of Sidi Bel-Abbes, Algeria

**Abstract:** The adhesive bonding technique is employed from the aeronautical/aerospace industry to current house products. To comply with the requirements of distinct applications, different joint configurations are available to the designer. While single-lap joints (SLJ) are the most common in application and research, double-lap joints, scarf joints and *T*-joints find specific applications. *T*-joints are seldom studied in the literature, but these are used, for instance, in aircraft to bond the stiffener beams to the skin, or in the cars between the *B*-pillar and the rocker. Due to the high stress concentrations, *T*-joints often fail under average stresses much lower than the adhesive strengths, giving rise to the necessity for proper design and strength improvement methodologies. This work initially aims to validate the cohesive zone modelling (CZM) technique with experiments, and then use it to numerically evaluate and optimize the performance of *T*-joints subjected to peel loads. CZM is nowadays regarded as the most powerful strength prediction tool for adhesive joints, and can be a valuable tool to improve *T*-joints. Different features are addressed for a complete analysis: adhesive type, geometrical parameters, dual-adhesive technique for strength improvement, and composite joints. The evaluated geometrical parameters are the base adherend thickness (*a*), *T*-part thickness (*t*), overlap or bonding length (*l*) and curvature radius (*r*). As a result of this work, the model was successfully validated, and clear design guidelines were provided to define the ideal geometric and material (adhesive) conditions for best performance.

**Keywords:** Polymeric material, adhesive joint, joint design, cohesive zone model, *T*-joint.

## 1. INTRODUCTION

Currently, polymers are commonly used as adhesive materials in different fields of knowledge, and adhesive joint design is a hot-topic in the academia. Adhesive bonding technology has several advantages in comparison with traditional joining methods such as bolting or welding, namely the improved stress fields, capacity to join different material types without compromising their integrity (e.g., absence of welding and hole drilling in composites), vibration reduction, and sealing [1]. Limitations of adhesive bonding include surface treatment necessity before applying the adhesive, typical disassembly difficulties, limited temperature and humidity, and appearance of undesired peel ( $\sigma_y$ ) stresses [2]. Between varying joint designs that the designer can choose from, the most simple and common for application and research purposes is the SLJ [3]. Other joining strategies consist of double-lap, scarf, stepped-lap, *T*, and tubular joints. The *T*-joint configuration finds application in different scenarios, including aviation, to bond stiffeners to the aircraft skin, and automotive industry, for the pillar-to-rocker connection. A common *T*-joint design joins a

base adherend to the *T*-part along a certain bonding length. The *T*-joint's main purpose is the transfer of peel loads between the base panel and the web [4]. Irrespectively of the bonded joint configuration, techniques are available in the literature for strength improvement, leading to improved load transfer and efficiency, by reducing stress concentrations and increasing the average stress at failure, including finding the optimal *l*, *a* and the adhesive thickness ( $t_a$ ) [5], applying adhesive fillets [6] and chamfers [7], and using the dual-adhesive technique [8]. The bi- or dual-adhesive technique is an invention of Raphael [9], and it consists of combining a low-stiffness adhesive at the highly-stressed overlap edges, with a high-stiffness adhesive at the inner overlap, typically under low stresses, aiming to make stress distributions more uniform and thus increase the joint strength.

To enable the design and application of adhesive bonding technology in different applications, it is necessary to accurately predict the adhesive joints' strength, which highly facilitates tailoring a specific solution to a given application without extensive experimental testing. Strength prediction of adhesive joints began with analytical models, e.g., the work of Hart-Smith [10], which were proposed to evaluate the joint performance. However, these techniques failed to

\*Address correspondence to this author at the INEGI – Pólo FEUP, Rua Dr. Roberto Frias, s/n, 4200-465 Porto, Portugal; Tel: +351939526892; Fax: +351228321159; E-mail: raulcampilho@gmail.com

work for novel ductile and tough adhesives. Finite element method (FEM) analyses, on the other hand, find accuracy for complex geometrical and material problems. With this approach, it becomes possible to account for virtually all possible effects and constraints necessary for the accurate assessment of the joints' behaviour. Continuum mechanics is the simplest approach, by considering the maximum stresses, strains or strain energy given by the models (or analytical approach), and comparing with the adhesive mechanical properties to predict failure [11]. Fracture mechanics assumes that structures and adhesives layers can have discontinuities and cracks, and that these can grow if specific conditions are met. CZM is a powerful approach to describe damage growth along the cohesive process zone leading to total detachment of the constituent parts of a structure. By CZM, damage can propagate along pre-defined paths established by the modeller. However, CZM relies on accurately estimated cohesive strengths in tension and in shear ( $t_n^0$  and  $t_s^0$ , respectively), and fracture toughnesses in mode I and II ( $G_{IC}$  and  $G_{IIC}$ , respectively). The extended finite element method (XFEM) is a more recent addition to the pool of available methods [12], additionally enabling to propagate cracks along arbitrary paths, unlike CZM. By XFEM, the mesh does not need to match the discontinuities, nor it is necessary to remeshing the model in the crack vicinity.

Adhesively-bonded *T*-joints are a less common topic of research in the literature, compared to simpler geometries, but few authors have addressed this geometry. The work of Zhan *et al.* [13] used damage mechanics to evaluate different *T*-joint configurations under tensile loads. The joint materials consisted of 2060-T8 aluminium alloy and the two-part epoxy adhesive EA9394. The experimental tests carried out positively validated the proposed numerical approach. The maximum load ( $P_m$ ) increased for higher bonding areas, and the horizontal bondline was more effective in the contribution to  $P_m$  than the vertical bondline. Actually, by considering a vertical bonding in a *T*-joint, the  $P_m$  increase was negligible, although the bondline increased by 123%. In a different work [14], CZM was used to address the adhesive type and geometry effects on the bending characteristics of *T*-joints. The joints were made of carbon-epoxy (IM7/8552) and glass-epoxy (E-glass/Epon 828) adherends. The joint strength depended on the applied adhesive and gave the following results (from best to worst): Araldite® AV138, Araldite® 2015, SikaForce® 7752, Cytec FM73 and Cytec FM300. *T*-joints with sharper corners led to the highest stresses at the respective vicinity and

smaller stresses at the overlap ends, while rounded corners promote the opposite behaviour. Higher stringer lengths diminish von Mises stresses at the bond ends, although the corner stresses increased. By increasing the web and stringer thickness increases von Mises stresses in the adhesive. Ramezani *et al.* [15] experimentally analysed the dual-adhesive technique in SLJ by employing digital image correlation (DIC). The analysis comprised a flexible and a stiff adhesive, and different geometries, by varying  $l$ ,  $a$  and  $t_a$ . DIC clarified the influence of these conditions on strain distributions, showing that, by increasing the applied load, the maximum compressive strains tend to approach the adhesives' interface. Compared to the single-adhesive joint, the dual-adhesive revealed higher strength.

This work initially aims to validate the CZM technique with experiments, and then use it to numerically evaluate and optimize the performance of *T*-joints subjected to peel loads. CZM is nowadays regarded as the most powerful strength prediction tool for adhesive joints, and can be a valuable tool to improve *T*-joints. Different features are addressed for a complete analysis: adhesive type, geometrical parameters, dual-adhesive technique for strength improvement, and composite joints.

## 2. MATERIALS AND METHODS

### 2.1. Description of *T*-Joint Models

The *T*-joint geometry is shown in Figure 1, and it consists of a double-*L* arrangement forming a *T*, using two bent parts bonded in their length. The *T*-joint includes a material-free portion at the radius region, between the double-*L* parts. A peel displacement was applied at the *T*-part edge, while the base (flat) adherend was clamped at both edges. The base dimensions are the following (all dimensions are given in mm): total length  $l_t=200$ , *T*-part height  $l_a=40$ ,  $l=30$ ,  $a=3$ ,  $t=1, 2, 3$  and  $4$ ,  $r=6$ ,  $t_A=0.2$ , and width  $b=25$ . On the other hand, the effect of geometric parameters is assessed through the comparative evaluation to the base geometry. The following configurations are tested (dimensions in mm):  $a$  (1, 2, 3 and 4),  $t$  (0.5, 1, 1.5, 2 and 2.5),  $l$  (10, 20, 30 and 40) and  $r$  (3, 6, 9 and 12).

### 2.2. Adherends and Adhesives

The *T*-joint analysis was mainly conducted with AW 6082-T651 aluminium alloy adherends (base adherend and *T*-part), with carbon-epoxy adherends being analysed in a 2<sup>nd</sup> stage. This aluminium alloy was

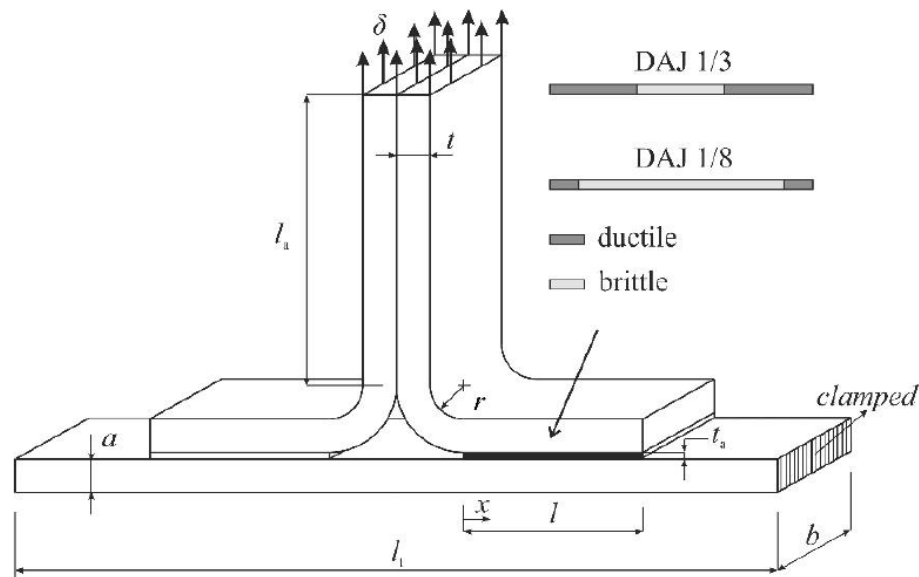


Figure 1: T-joint geometry.

previously tested [16], leading to the mechanical properties: Young's modulus ( $E$ ) of  $70.07 \pm 0.83$  GPa, tensile yield stress ( $\sigma_y$ ) of  $261.67 \pm 7.65$  MPa, tensile strength ( $\sigma_f$ ) of  $324 \pm 0.16$  MPa and tensile failure strain ( $\varepsilon_f$ ) of  $21.70 \pm 4.24\%$ . On the other hand, the carbon-epoxy adherends are made of unidirectional prepreg plates with carbon fibre reinforcement and epoxy matrix (SEAL<sup>®</sup> Texipreg HS 160 RM; Legnano, Italy). The ply unit thickness of the prepreg is 0.125 mm, and manual fabrication consisted of hand lay-up and curing in a press during 1 h at  $130^\circ\text{C}$  and 2 bar pressure. The elastic orthotropic data for a single unidirectional lamina, required for the numerical models, are described in a previous work [17]. The work is mainly conducted with the ductile epoxy adhesive Araldite<sup>®</sup>

2015, but a total of three adhesives were used, namely for the adhesive type and dual-adhesive analyses. The Araldite<sup>®</sup> AV138 is a brittle epoxy adhesive, and the Sikaforce<sup>®</sup> 7752 is a ductile polyurethane adhesive. The collected properties are described in Table 1. All properties were defined in previous research works, providing the necessary information for CZM modelling. The tensile bulk data ( $E$ ,  $\sigma_y$ ,  $\sigma_f$  and  $\varepsilon_f$ ) resulted from bulk tests to dog bone specimens. The shear properties were acquired using thick-adherend shear tests (TAST) on bonded steel specimens. The tensile and shear fracture data were found by performing Double-Cantilever Beam and End-Notched Flexure tests, respectively.

Table 1: Properties of the Adhesives Araldite<sup>®</sup> AV138 [18], Araldite<sup>®</sup> 2015 [19] and SikaForce<sup>®</sup> 7752 [20].

Property	AV138	2015	7752
Young's modulus, $E$ [GPa]	$4.9 \pm 0.8$	$1.9 \pm 0.2$	$0.5 \pm 0.1$
Poisson's ratio, $\nu$	0.35 <sup>a</sup>	0.33 <sup>a</sup>	0.30 <sup>a</sup>
Tensile yield stress, $\sigma_y$ [MPa]	$36.5 \pm 2.5$	$12.6 \pm 0.6$	$3.2 \pm 0.5$
Tensile failure strength, $\sigma_f$ [MPa]	$39.5 \pm 3.2$	$21.6 \pm 1.6$	$11.5 \pm 0.3$
Tensile failure strain, $\varepsilon_f$ [%]	$1.2 \pm 0.1$	$4.8 \pm 0.2$	$19.2 \pm 1.4$
Shear modulus, $G$ [GPa]	$1.6 \pm 0.0$	$0.6 \pm 0.2$	$0.2 \pm 0.0$
Shear yield stress, $\tau_y$ [MPa]	$25.1 \pm 0.3$	$14.6 \pm 1.3$	$5.2 \pm 1.1$
Shear failure strength, $\tau_f$ [MPa]	$30.2 \pm 0.4$	$17.9 \pm 1.8$	$10.2 \pm 0.6$
Shear failure strain, $\gamma_f$ [%]	$7.8 \pm 0.7$	$43.9 \pm 3.4$	$54.8 \pm 6.4$
Toughness in tension, $G_{IC}$ [N/mm]	0.2 <sup>b</sup>	$0.4 \pm 0.0$	$2.4 \pm 0.2$
Toughness in shear, $G_{IIC}$ [N/mm]	0.4 <sup>b</sup>	$4.7 \pm 0.3$	$5.4 \pm 0.5$

<sup>a</sup>manufacturer's data.

### 2.3. Model Pre-Processing

CZM was applied to infer the  $T$ -joint peel performance, after validation with experimental results, taking advantage of the Abaqus<sup>®</sup> software and the built-in CZM module. Only half model was considered, by applying symmetry conditions, aiming to reduce the computational load associated to the static analyses carried out for the different joint configurations. The models were built as two-dimensional (2D) due to the constant shape along the width, and the geometry partitioning technique facilitates the mesh construction by reducing element distortions. The aluminium and carbon-epoxy adherend partitions were populated by solid elements with 4 nodes and plane-strain formulation (CPE4 elements) [18]. The thin adhesive layer was modelled using a single row of CZM elements (COH2D4 elements with 4 nodes). Figure 2 shows a mesh example.

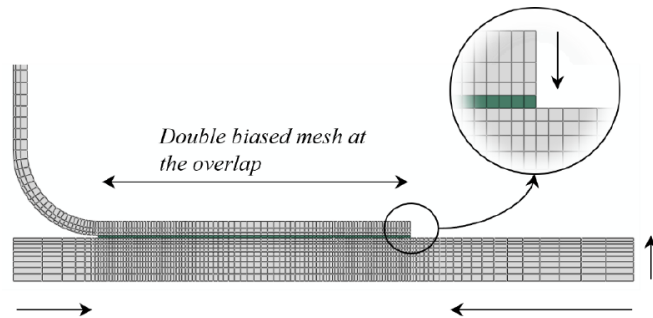


Figure 2: Mesh refinement for the  $T$ -joint with  $t=1$  mm.

A cohesive-type section was applied in the adhesive layer, with geometry defined thickness. All aluminium alloy and carbon-epoxy sections were considered as solid and homogeneous. Application of the boundary conditions involved clamping the base adherend edge and vertically pulling the  $T$ -part with a prescribed displacement at its top edge. Vertical symmetry conditions were applied in all models. To simulate decohesion, a triangular-shape CZM was applied in the adhesive layer, which included a mixed-mode formulation involving a quadratic stress criterion to assess damage initiation and a linear power-law energetic criterion to deal with crack propagation. The detailed description of the CZM model is given in reference [21]. The adhesives' data for the simulations are those of Table 1.

### 3. RESULTS

The results section is divided into the CZM validation, to enable numerical application of the procedure to different analyses, followed by a purely

numerical  $P_m$  analysis on different  $T$ -joint features: adhesive type (AV138, 2015, and 7752), geometrical parameters ( $a$ ,  $t$ ,  $l$ , and  $r$ ), dual adhesive technique, and composite adherends.

#### 3.1. CZM Validation

Initially, CZM validation is carried out with the  $T$ -joint geometry depicted in Figure 1, aluminium alloy adherends and the 2015. For fabrication, the adherends were initially cut and bent to the  $L$ -shape. Surface preparation for bonding consisted of grit blasting and cleaning with acetone. The adhesive was then poured into the surfaces to join, and the assembly cured in a jig that assured the joint alignment. The desired  $t_a$  was assured with calibrated steel spacers. Pressure was applied individually to each specimen with grips [22]. The joints were cured over a one-week period and, finally, the excess adhesive resulting from the fabrication process removed by trimming. Testing was accomplished at least one week after assembly, and executed at room temperature and velocity of 1 mm/min to emulate static test conditions, in a Shimadzu AG-X 100 machine. A total five repetitions were considered for each joint configuration, defined by  $t$  (Figure 1). Visual observation to the failed specimens showed cohesive failures of the adhesive for all  $t$  and repetitions. Figure 3 summarizes the collected experimental  $P_m$  data and the respective numerical predictions.

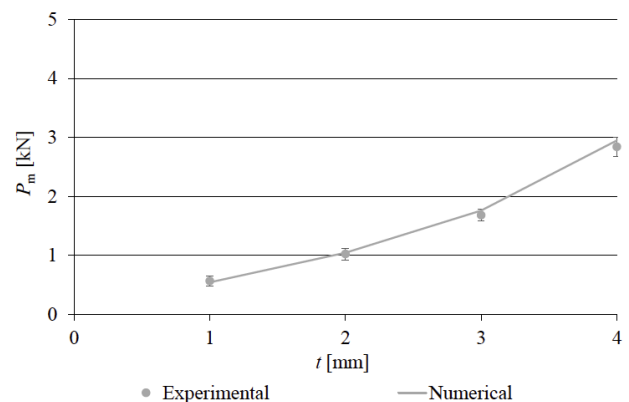


Figure 3: Experimental and numerical  $P_m$  vs.  $t$  data.

Analysis to the experimental  $P_m$  reveals a clear  $t$  effect with benefit of higher  $t$ , especially between 3 and 4 mm. Considering the validation adhesive (2015), and compared to the base geometry with  $t=1$  mm, the percentile  $P_m$  improvements for consecutive  $t$  increases up to 4 mm are 81.2%, 197.8% and 403.7%, thus showing a significant effect of the  $T$ -part stiffness on the joint performance. Previous analyses showed that this difference is due to the reduction of  $\sigma_y$  and shear

( $\tau_{xy}$ ) peak stresses [23]. Additionally, this adhesive can plasticize before failure, which enables a larger region of stress transfer by increasing  $t$ . The CZM  $P_m$  predictions showed a good match to the experiment data, although  $P_m$  was always predicted by excess of the experimental average values, except for 1 mm (4.3% difference by default). For  $t=2, 3$  and 4 mm, the experimental  $P_m$  was under the numerical predictions by 2.2%, 4.5% and 3.5%, in this order. As a result of the validation process, the CZM technique can be considered reliable for the following numerical parametric analysis.

### 3.2. Adhesive Type

The initial analysed effect on the  $T$ -joints'  $P_m$  behaviour is the adhesive type, considering the three adhesives described in section 2.2. For this and the subsequent analyses, the  $P_m$  data is collected from the load-displacement ( $P-\delta$ ) curves resulting from the numerical simulations, which is also used to analyse stress distributions and failure modes. Figure 4 shows that higher  $l$  improves  $P_m$  in  $T$ -joints bonded with ductile adhesives, i.e., 2015 and 7752. On the other hand, this improvement was not possible by using the AV138, due to its inherent brittleness, and no sensible variations in  $P_m$  are detected in the plot. For this adhesive,  $P_m$  actually diminishes from 1473 N to 1471 N between  $l=10$  and 40 mm. As a totally opposite behaviour, the  $T$ -joints bonded with the 7752, which is the most ductile of the three adhesives, suffered a  $P_m$  improvement from 3452 N to 5878 N between  $l=10$  and 40 mm (70.3% difference). It is possible to conclude from this analysis that ductile adhesives accomplish significant  $P_m$  improvements, since these adhesives are able to absorb and plasticize at the locations of peak stresses before reaching failure, thus providing a major advantage over stronger but brittle adhesives, which in this geometry do not work well due to the predominant peel load.

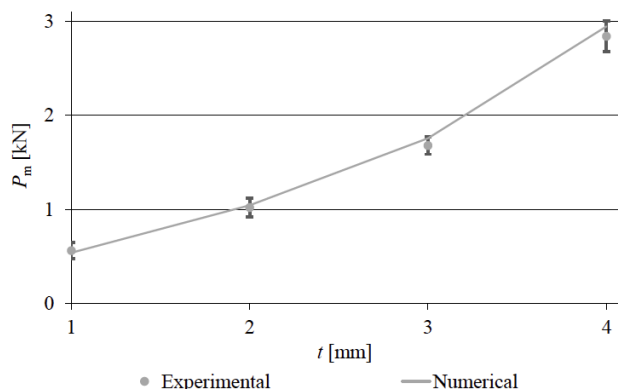


Figure 4: Adhesive type effect on  $P_m$ .

### 3.3. Geometrical Parameters

Different geometrical parameters are also addressed for the base adhesive (2015), supported by the presented  $P_m$  data in Figure 5. Each parameter is addressed individually:

- The  $a$  parameter highly affects  $P_m$ , with benefit of higher  $a$  (Figure 5a). Between  $a=1$  and 4 mm, the  $P_m$  increase was significant (by 112.8%), and it is justified by the deflection reduction of the base, which makes stress distributions more uniform. In the opposite direction, higher  $a$  values reduce the allowable displacement of the joints before failure. On the other hand, increasing  $a$  decreases the failure displacement;
- Higher  $t$  has an identical effect to  $a$ , i.e.,  $P_m$  increases with  $t$  (Figure 5b). A 30.8 %  $P_m$  improvement was found by increasing  $t$  from 0.5 to 2.5 mm. Nonetheless, for  $t=1.5$  mm a short disruption to this tendency was found. The numerical analysis showed that  $\sigma_y$  and shear ( $\tau_{xy}$ ) stresses increased at the bond edges and that the failure mode changed by comparing  $t=0.5$  and  $t=1$  mm with  $t=1.5, 2$  and 2.5 mm, leading to the inconsistent  $P_m$  evolution. In the first scenario, failure took place at the curvature radius region, while in the second scenario it occurred at the bond edges. The failure displacement slightly increased for higher  $t$ ;
- $P_m$  steadily increases with  $l$ , with preponderance for higher  $l$  (Figure 5c). The relative improvement between limit  $l$  was 112.2%. A detailed analysis showed that, for this adhesive, higher  $l$  enable plasticization at the stress concentration regions, leading to  $P_m$  improvements due to higher average stresses and higher bonded areas. The failure displacement increased with  $l$  as well;
- The  $r$  effect is depicted in Figure 5d, showing a linear increase of  $P_m$  by reducing  $r$  (difference of 17.2% between the limit  $r$  values). It was found that this variation was caused by alterations in  $\sigma_y$  and  $\tau_{xy}$  stresses at the radius vicinity. The displacement at joint failure also decreased for higher  $r$ .

### 3.4. Dual Adhesives

Figure 6 presents the  $P_m-t$  data considering the 2015, 7752, and 7752-2025-7752 (dual-adhesive) joints. It is clear that the dual-adhesive joint can

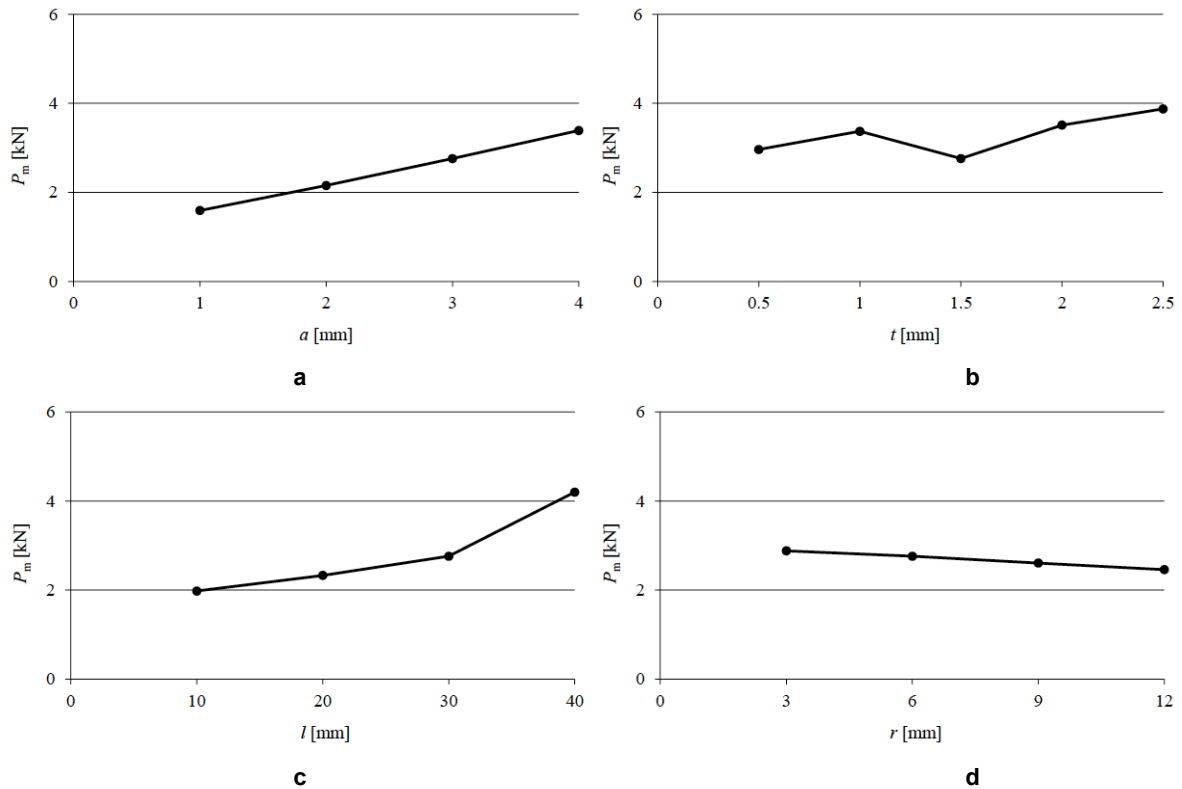


**Figure 5:** Geometrical parameter effect on  $P_m$ : influence of  $a$  (a),  $t$  (b),  $l$  (c) and  $r$  (d).

perform better than a single-adhesive joint in the  $T$ -joint configuration, but the joint geometry should be carefully chosen. Between all tested joints, those bonded with the 2015 provide the most modest  $P_m$  results. Thus, the associated  $P_m$  data points are the benchmark of the complete data pool. Between the two considered adhesives for this analysis, the 2015 is stronger than the 7752 (Table 1). However, the 7752 ductility largely exceeds that of the 2015. Since  $T$ -joints have a predominant peel load, and significant peak stresses are present in the adhesive layer, the 7752 is able to sustain higher loads before failure, thus leading to improved  $P_m$ . Table 2 quantifies the differences between all joints, and evaluates  $\Delta P_m$  (variation of  $P_m$  to the single-adhesive  $T$ -joint bonded with the 2015). The  $T$ -joint bonded with the 7752 manages to provide  $\Delta P_m$  up to 38%, for  $t=1$  mm, which corroborates the former discussion. The advantage of the dual adhesive joint technique varies according to  $t$ , and also to the adhesives' proportion. Considering the dual-adhesive joint 1/8, real advantage over the 7752 is restricted to  $t=3$  mm, in which case  $\Delta P_m$  reaches 20%. On the other hand, the dual-adhesive joint 1/3 clearly performs best between all tested conditions (single- or dual-adhesive), even though, for  $t=1$  mm,  $\Delta P_m$  is identical to the single-adhesive joint with the 7752. Between all  $t$ , the highest  $\Delta P_m$  corresponded to  $t=1$  mm and reached

38%.  $\Delta P_m$  values were less significant for the remaining  $t$ , but the variations to the single-adhesive joints bonded with the 2015 and 7752 cannot be disregarded as well. Comparison of the best solution between all  $t$  shows that this variable is relevant for joint design, and the best  $P_m$  result corresponds to  $t=3$  mm.

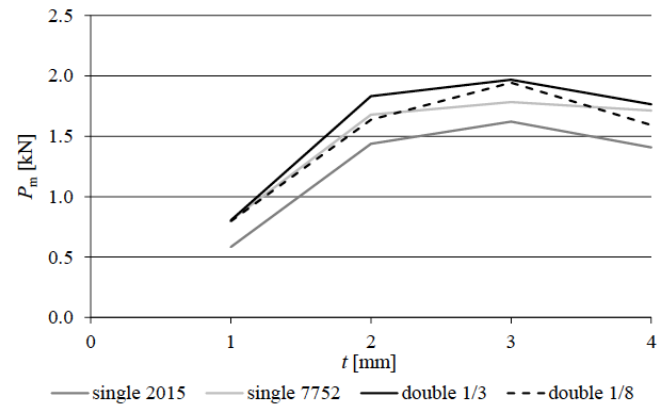


**Figure 6:** Dual-adhesive effect on  $P_m$ .

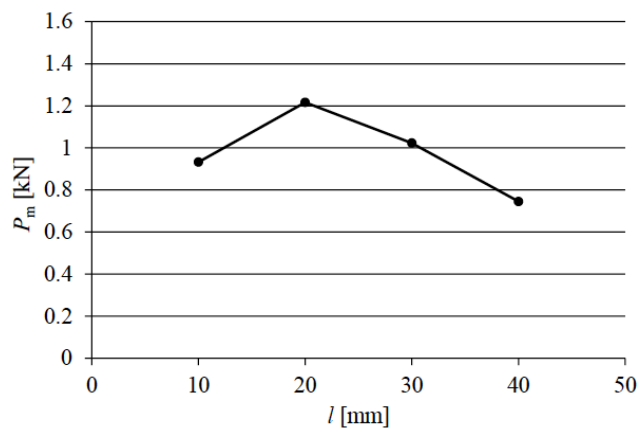
### 3.5. Composite Adherends

The  $T$ -joint geometry depicted in Figure 1 is addressed as a function of  $l$ . Although different failure paths were considered in the numerical models (including composite failures), typically fracture was cohesive in the adhesive. The numerical  $P_m$ - $l$  data are

**Table 2: Collected  $P_m$  and  $\Delta P_m$  Data for the Dual-Adhesive Joint Analysis**

Adhesive	$t$ (mm)	1	2	3	4
2015		582.65 N	1437.4 N	1621.86 N	1407.29 N
7752		803.91 N (38%)	1678.74 N (17%)	1782.81 N (10%)	1712.64 N (22%)
Dual-adhesive joint 1/8		796.18 N (37%)	1636.25 N (14%)	1943.46 N (20%)	1592.09 N (13%)
Dual-adhesive joint 1/3		803.94 N (38%)	1832.58 N (27%)	1968.68 N (21%)	1764.87 N (25%)

provided in Figure 7. It is found that  $P_m$  increases with  $l$  from 10 to 20 mm, although further increasing  $l$  leads to a strength depreciation. The relative variations of  $P_m$ , compared against the base geometry with  $l=10$  mm, were calculated as +30.5%, +9.7%, and -20.1% for increasing  $l$  up to 40 mm. A detailed analysis of the software model showed that  $\sigma_y$  and  $\tau_{xy}$  peak stresses at the bond edges tend to increase with  $l$ , due to the increased stiffness of the bonded set, which may cancel the theoretical advantage in having a bigger area of adhesive by increasing  $l$ . In the current case, it was actually found that the  $P_m$  disruption has origin on a modification of the failure mode. Up to  $l=20$  mm failures were cohesive in the adhesive layer, while above  $l=20$  mm the radius region failed prematurely to cohesive failure of the adhesive, obstructing higher  $P_m$  and leading to the reported behaviour. Moreover, and differently to what is known to occur for SLJ, for instance, this failure mode alteration effectively reduced  $P_m$  over a geometry with less bonded area.

**Figure 7: Material effect on  $P_m$ .**

#### 4. CONCLUSIONS

The present work was accomplished to optimize aluminium alloy  $T$ -joints under peel loads, using CZM, after validation  $T$  with experiments. The analysis comprised different adhesives, geometric variables ( $a$ ,  $t$ ,  $l$  and  $r$ ), dual-adhesive technique, and composite adherends. The numerical analysis was carried out in

Abaqus<sup>®</sup>. Validation was initially positively done, which enabled the subsequent numerical approach. The following conclusions are divided into these four approaches:

- Adhesive type: the 7752 provided the highest  $P_m$  disregarding  $l$ , showing a major improvement up to  $l=20$  mm. This behaviour is justified by the plasticization allowance at the adhesive edges, even though the adhesive is the least strong between the three adhesives. Applying the AV138 showed no advantage to higher  $l$  because of the loading nature. The 2015 has intermediate properties and showed a smaller  $P_m$  evolution than the 7752;
- Geometrical parameters:
  - Higher  $a$  linearly increased  $P_m$  on account of resulting in a stiffer base and less deflection. This parameter was found to be highly relevant for the joint behaviour;
  - Increasing  $t$  promotes a  $P_m$  improvement in the considered range, apart from the  $T$ -joint with  $t=1.5$  mm due to modification of the failure mode;
  - Increasing  $l$  provides higher bonded area, which increases  $P_m$ , with preponderance for higher  $l$ ;
  - $P_m$  increases linearly with the  $r$  reduction due to stress field modifications in the adhesive.
- Dual adhesives: the  $T$ -joints mostly failed between the two adhesives in the bondline, despite variations with  $t$ . The dual-adhesive joint (1/3) provides the best results, and it is possible to obtain relevant  $P_m$  improvements over single-adhesive joints;
- Composite adherends: higher  $l$  increase  $P_m$  up to 20 mm. For higher  $l$ , lead to a failure mode modification that actually reduce the joint performance.

**DECLARATION OF COMPETING INTEREST**

The authors declare no conflict of interest.

**REFERENCES**

- [1] Petrie EM. Handbook of adhesives and sealants. New York, USA: McGraw-Hill, 2000.
- [2] Da Silva LF, Öchsner A and Adams RD. Handbook of adhesion technology. Springer Science & Business Media, 2011.  
<https://doi.org/10.1007/978-3-642-01169-6>
- [3] Adams RD. Adhesive bonding: science, technology and applications. Elsevier, 2005.  
<https://doi.org/10.1533/9781845690755>
- [4] Li W, Blunt L and Stout KJ. Analysis and design of adhesive-bonded tee joints. *Int J Adhes Adhes* 1997; 17: 303-311.  
[https://doi.org/10.1016/S0143-7496\(97\)00012-2](https://doi.org/10.1016/S0143-7496(97)00012-2)
- [5] Oliveira JGG, Campilho RDSG, Silva FJG, et al. Adhesive thickness effects on the mixed-mode fracture toughness of bonded joints. *J Adhes* 2019; 1-21.  
<https://doi.org/10.1080/00218464.2019.1681269>
- [6] Luo H, Yan Y, Zhang T, et al. Progressive failure and experimental study of adhesively bonded composite single-lap joints subjected to axial tensile loads. *J Adhes Sci Technol* 2016; 30: 894-914.  
<https://doi.org/10.1080/01694243.2015.1131806>
- [7] Moya-Sanz EM, Ivañez I, Garcia-Castillo SK. Effect of the geometry in the strength of single-lap adhesive joints of composite laminates under uniaxial tensile load. *Int J Adhes Adhes* 2017; 72: 23-29.  
<https://doi.org/10.1016/j.ijadhadh.2016.10.009>
- [8] Ferreira CL, Campilho R and Moreira RDF. Experimental and numerical analysis of dual-adhesive stepped-lap aluminum joints. *P I Mech Eng E-J Pro* 2020; 234: 454-464.  
<https://doi.org/10.1177/0954408920905747>
- [9] Raphael C. Variable-adhesive bonded joints (Stresses in ordinary lap joint compared to variable adhesive joint). In: *Structural Adhesives Bonding Symposium* Hoboken, USA, 1966, pp.99-108.
- [10] Hart-Smith LJ. Adhesive-bonded single-lap joints. NASA Contract Report, NASA CR-112236, 1973.
- [11] Da Silva LF and Campilho RD. Advances in numerical modelling of adhesive joints. *Advances in numerical modeling of adhesive joints*. Springer, 2012, pp.1-93.  
[https://doi.org/10.1007/978-3-642-23608-2\\_1](https://doi.org/10.1007/978-3-642-23608-2_1)
- [12] Belytschko T and Black T. Elastic crack growth in finite elements with minimal remeshing. *Int J Numer Methods Eng* 1999; 45: 601-620.  
[https://doi.org/10.1002/\(SICI\)1097-0207\(19990620\)45:5<601::AID-NME598>3.0.CO;2-S](https://doi.org/10.1002/(SICI)1097-0207(19990620)45:5<601::AID-NME598>3.0.CO;2-S)
- [13] Zhan X, Gu C, Wu H, et al. Experimental and numerical analysis on the strength of 2060 Al-Li alloy adhesively bonded T joints. *Int J Adhes Adhes* 2016; 65: 79-87.  
<https://doi.org/10.1016/j.ijadhadh.2015.11.010>
- [14] Barzegar M, Moallem MD and Mokhtari M. Progressive damage analysis of an adhesively bonded composite T-joint under bending, considering micro-scale effects of fiber volume fraction of adherends. *Compos Struct* 2021; 258: 113374.  
<https://doi.org/10.1016/j.compstruct.2020.113374>
- [15] Ramezani F, Ayatollahi MR, Akhavan-Safar A, et al. A comprehensive experimental study on bi-adhesive single lap joints using DIC technique. *Int J Adhes Adhes* 2020; 102: 102674.  
<https://doi.org/10.1016/j.ijadhadh.2020.102674>
- [16] Moreira RDF and Campilho RDSG. Strength improvement of adhesively-bonded scarf repairs in aluminium structures with external reinforcements. *Eng Struct* 2015; 101: 99-110.  
<https://doi.org/10.1016/j.engstruct.2015.07.001>
- [17] Ribeiro F, Campilho R, Carbas R, et al. Strength and damage growth in composite bonded joints with defects. *Compos B Eng* 2016; 100: 91-100.  
<https://doi.org/10.1016/j.compositesb.2016.06.060>
- [18] Campilho RDSG, Banea MD, Pinto AMG, et al. Strength prediction of single- and double-lap joints by standard and extended finite element modelling. *Int J Adhes Adhes* 2011; 31: 363-372.  
<https://doi.org/10.1016/j.ijadhadh.2010.09.008>
- [19] Campilho RD, Banea MD, Neto J, et al. Modelling adhesive joints with cohesive zone models: effect of the cohesive law shape of the adhesive layer. *Int J Adhes Adhes* 2013; 44: 48-56.  
<https://doi.org/10.1016/j.ijadhadh.2013.02.006>
- [20] Faneco T, Campilho R, Silva F, et al. Strength and fracture characterization of a novel polyurethane adhesive for the automotive industry. *J Test Eval* 2017; 45: 398-407.  
<https://doi.org/10.1520/JTE20150335>
- [21] Campilho RDSG, Banea MD, Neto JABP, et al. Modelling of single-lap joints using cohesive zone models: Effect of the cohesive parameters on the output of the simulations. *J Adhes* 2012; 88: 513-533.  
<https://doi.org/10.1080/00218464.2012.660834>
- [22] Campilho RDSG, Banea MD, Chaves FJP, et al. eXtended Finite Element Method for fracture characterization of adhesive joints in pure mode I. *Comput Mater Sci* 2011; 50: 1543-1549.  
<https://doi.org/10.1016/j.commatsci.2010.12.012>
- [23] Carneiro MAS and Campilho RDSG. Analysis of adhesively-bonded T-joints by experimentation and cohesive zone models. *J Adhes Sci Technol* 2017; 31: 1998-2014.  
<https://doi.org/10.1080/01694243.2017.1291320>

Received on 08-03-2023

Accepted on 05-04-2023

Published on 20-04-2023

<https://doi.org/10.6000/1929-5995.2023.12.03>

© 2023 Lopes et al.; Licensee Lifescience Global.

This is an open access article licensed under the terms of the Creative Commons Attribution License (<http://creativecommons.org/licenses/by/4.0/>) which permits unrestricted use, distribution and reproduction in any medium, provided the work is properly cited.